Optimal fold symmetry of LH2 rings on a photosynthetic membrane

Liam Cleary, Hang Chen, Chern Chuang, Robert J. Silbey[1], and Jianshu Cao[2]

Department of Chemistry, Massachusetts Institute of Technology, Cambridge, MA 02139

Edited by Michael L. Klein, Temple University, Philadelphia, PA, and approved March 12, 2013 (received for review October 18, 2012)

An intriguing observation of photosynthetic light-harvesting systems is the *N*-fold symmetry of light-harvesting complex 2 (LH2) of purple bacteria. We calculate the optimal rotational configuration of *N*-fold rings on a hexagonal lattice and establish two related mechanisms for the promotion of maximum excitation energy transfer (EET). (*i*) For certain fold numbers, there exist optimal basis cells with rotational symmetry, extendable to the entire lattice for the global optimization of the EET network. (*ii*) The type of basis cell can reduce or remove the frustration of EET rates across the photosynthetic network. We find that the existence of a basis cell and its type are directly related to the number of matching points *S* between the fold symmetry and the hexagonal lattice. The two complementary mechanisms provide selection criteria for the fold number and identify groups of consecutive numbers. Remarkably, one such group consists of the naturally occurring 8-, 9-, and 10-fold rings. By considering the inter-ring distance and EET rate, we demonstrate that this group can achieve minimal rotational sensitivity in addition to an optimal packing density, achieving robust and efficient EET. This corroborates our findings *i* and *ii* and, through their direct relation to *S*, suggests the design principle of matching the internal symmetry with the lattice order.

Photosynthesis lies at the heart of all life on the planet. Excitation energy created in a peripheral light-harvesting antenna complex, upon absorption of a photon, is efficiently transferred via an exciton mechanism, sometimes over hundreds of angstroms, to a reaction center where charge separation takes place, creating a transmembrane electrochemical potential difference that ultimately drives the production of ATP. Light-harvesting antenna complexes, whose primary function is to increase the effective cross-section for photon absorption, while maintaining an efficient energy transfer network, consist of well-ordered membrane-associated arrays of light-absorbing pigments, namely chlorophyll or bacteriochlorophyll (BChl), embedded in a protein environment (1–4).

Perhaps the most intriguing aspect of light-harvesting systems is the *N*-fold symmetry displayed by light-harvesting complex 2 (LH2) of purple nonsulfur bacteria. Fold symmetry occurs in systems as diverse as carbon nanotubes, tubular dye aggregates, and the mosaic virus protein, as well as in snow flakes, tori, and nonperiodic tilings (5). In LH2, the *N*-fold symmetry arises from the *N* repetitions of a basic heterodimer subunit consisting of two transmembrane polypeptides, α and β, arranged in a circular structure (6–8). Each $\alpha\beta$-heterodimer subunit noncovalently binds one B800 BChl and two B850 BChls (Fig. 1*A*), so named according to their respective room-temperature absorption bands in the infrared region of the spectrum. In most bacterial species, the $\alpha\beta$-heterodimer repeats eight or nine times to form an octameric or nonameric ring structure (in *Rhodopseudomonas paulisterium* 10-fold rings have also been observed). Since the breakthrough of the first crystallizations of LH2 (9, 10), X-ray crystallography has determined the nine- and eightfold structures of *Rhodopseudomonas acidophila* and *Rhodospirillum molischianum*, respectively, to within a resolution of ~ 2 Å. Subsequent, equilibrium and nonequilibrium molecular dynamics simulations of their subunit heterodimers have shown that the mean values of separations between heterodimers are nearly fixed (11), so that the heterodimer subunit is independent of fold number. Consequently, a simple variation of the angle attained during self-assembly between heterodimers can achieve a complete ring of specific fold number *N*. This raises an important question, as to the role of specific fold symmetry in the highly efficient excitation energy transfer (EET) observed in light-harvesting complexes.

However, another intriguing aspect, in addition to the fold symmetry of the indvidual LH2 complexes, is the lattice structure evident in their supramolecular organization (12–14). Recent progress in atomic force microscopy (AFM), which allows direct observation of the bacterial photosynthetic complexes on their native membrane, has revealed that LH2 complexes occur in well-ordered hexagonal domains (Fig. 1*B*) (15–17). This is especially evident in bacterial membranes grown under low light intensity, where large LH2 domains, some hundreds of angstroms wide, form a hexagonal lattice to increase absorption. Not surprisingly, hexagonal order is the closest packing structure on a two-dimensional surface. An important observation is that well-ordered hexagonal domains occur for both octameric and nonameric structures, suggesting that a close packing order is preferable to a crystalline order. Understanding the symmetry properties on the level of both the individual complex and the supramolecular complex is necessary to form a complete picture of efficient excitation energy transfer in the light-harvesting antenna (18, 19) and has direct implications for the design of efficient synthetic devices (20–26).

In this work, we investigate the role of fold symmetry in promoting excitation energy transfer in LH2 hexagonal domains, using an *N*-fold model geometry of a B850 ring based on the $\alpha\beta$-heterodimer subunit of *Rps. acidophila* (outlined in *SI Materials and Methods*, Fig. S1). Considering the effective Hamiltonian of the *N*-fold geometry, and noting an important property of *N*-fold symmetric ring structures, namely the existence of $N-2$ and $N-1$ pairs of degenerate eigenstates for even and odd *N* (*SI Materials and Methods*), we arrive at a simple metric for determining the maximum excitation energy transfer rate between two B850 rings, based on the multichromophoric Förster theory (Eq. **6**). We first discuss the issues of symmetry and frustration on a hexagonal lattice and then explore the optimal rotational configuration of *N*-fold rings and establish two related fold symmetry mechanisms for the promotion of maximum excitation energy transfer. Using these mechanisms as selection criteria, we can identify groups of consecutive fold numbers. However, to understand why one consecutive group may be preferable to another we require additional considerations (the fold symmetry mechanisms effectively provide a prescreening of fold numbers). In particular, supposing an optimal packing density of heterodimers on the bacterial membrane,

Author contributions: R.S. and J.C. designed research; L.C., H.C., and C.C. performed research; and L.C., H.C., and J.C. wrote the paper.

The authors declare no conflict of interest.

This article is a PNAS Direct Submission.

[1]Deceased October 27, 2011.

[2]To whom correspondence should be addressed. E-mail: jianshu@mit.edu.

This article contains supporting information online at www.pnas.org/lookup/suppl/doi:10.1073/pnas.1218270110/-/DCSupplemental.

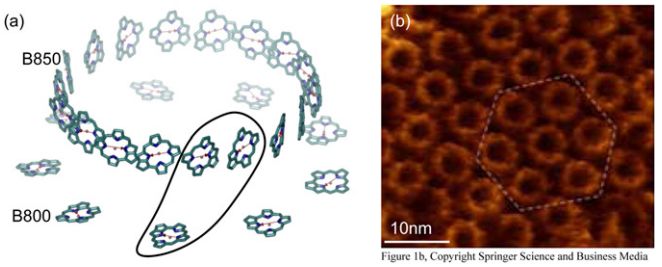

Fig. 1. (*A*) Structure of nonameric LH2 from *Rps. acidophila* with a single $\alpha\beta$-heterodimer subunit indicated. The transition dipoles (red arrows) are drawn from the N_B to N_D atoms of each BChl. (*B*) High-resolution AFM image of a low-light–adapted native membrane of *Rhodospirillum photometricum*, showing the hexagonal lattice structure. Reproduced with permission from Springer Science and Business Media (17).

we demonstrate how the consecutive group of 8-, 9-, and 10-fold rings appears preferable in nature by considering the inter-ring distance, the EET rate, and rotational sensitivity.

Results

Symmetry and Frustration. Before considering the optimal rotational configuration of LH2 rings of specific fold number, we first illustrate two basic physical properties of general *N*-fold rings on a hexagonal lattice, namely symmetry and frustration. The relationship between the internal *N*-fold symmetry of the LH2 ring and the external symmetry of an underlying hexagonal lattice can be demonstrated as follows. For any fold number *N*, we may find the number of matching points *S* with the hexagonal lattice by simply counting the number of rotations under which the B850 ring remains invariant with respect to the underlying lattice, i.e., the number of times *S* that $\mathrm{mod}(2\pi s'/6, 2\pi/N) = 0$ is true with $s' = 1, 2, \ldots, 6$ [or simply $S = \gcd(6, N)$]. This is illustrated in Fig. 2*A* for the cases of six-, four-, and threefold rings that have $S = 6$ $(0°, 60°, 120°, 180°, 240°, 300°)$, $S = 2$ $(0°, 180°)$, and $S = 3$ $(0°, 120°, 240°)$ matching points, respectively. The number of matching points indicates the degree of symmetry throughout the lattice of *N*-fold rings, with $S = 6$ indicating perfect matching between the *N*-fold ring and the hexagonal lattice. This has direct implications for the degree of dipole–dipole frustration throughout the lattice as follows.

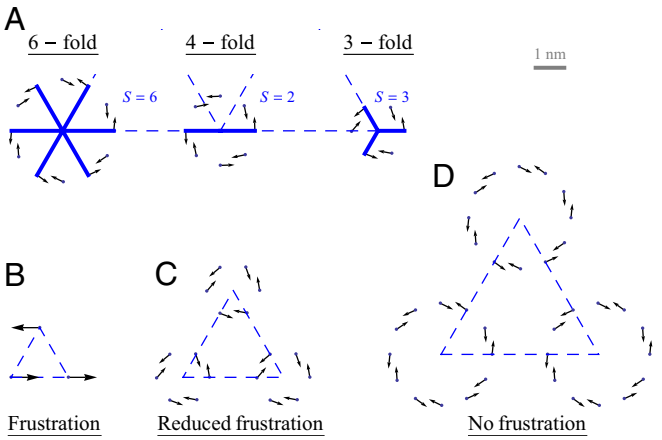

Fig. 2. (*A*) Number of matching points *S* (solid lines) for LH2 rings on a hexagonal lattice (dashed lines) with six-, four-, and threefold symmetry. Points and arrows represent the Mg atoms and accompanying transition dipoles. (*B*) Frustration of point dipoles. (*C* and *D*) Introducing *N*-fold symmetric aggregates of point dipoles can (*C*) reduce the degree of or (*D*) remove completely the dipole–dipole frustration.

Consider three point dipoles placed at the vertices of an equilateral triangle as in Fig. 2*B*. Upon maximizing the coupling between the three dipoles as a function of their rotation angles, one finds that the maximum coupling is not equal to the sum of the three pairwise maximum couplings; i.e., $|V|^2_{3\mathrm{dipoles}} \neq |V|^2_{12\mathrm{max}} + |V|^2_{23\mathrm{max}} + |V|^2_{31\mathrm{max}}$ (subscripts denote the pair of point dipoles). This is known as dipole–dipole frustration and is a consequence of the imposition of the underlying lattice structure. This frustration, however, can be reduced or removed by introducing aggregates of dipoles in place of point dipoles. In particular, as shown in Fig. 2 *C* and *D*, placing three- and sixfold symmetric rings (with $S = 3$ and $S = 6$, respectively) at the vertices reduces and removes the frustration, respectively. Thus, the degree of dipole–dipole frustration on the hexagonal lattice depends on the fold symmetry *N* via the number of matching points *S*. As we shall see, this is exactly the case when one considers the EET between rings placed on a hexagonal lattice, so that the frustration of EET rates can be reduced or removed as a function of *N*. Having briefly introduced the issues of symmetry mismatch and its implications for EET frustration, we now consider the role of fold symmetry in optimizing EET for nine- and eightfold LH2 rings.

Ninefold B850 Rings. Placing two identical ninefold rings at a center-to-center distance of $d_c = 75$ Å (corresponding to an inter-ring distance of $d = 21.8$ Å), in Fig. 3*A* we plot the dependence of the EET rate as measured by its effective dipolar coupling $|J|^2_{12}$ (subscripts denote the pair of rings), given by Eq. **6** below, on the rotation angles θ_1 and θ_2 of the two rings. The maximum EET rate occurs at $(\theta_1, \theta_2) = (13°, 33°)$. Note that the mirror symmetry lines (Fig. 3*A*, dashed lines), which pass through the maximum and minimum, occur at $\theta_1 = \theta_2 \pm \pi/9$ and that the dependence is $2\pi/9$ periodic (compare Fig. 3*B*). Both observations are directly related to the fold symmetry. In fact, a simple geometrical argument (*SI Materials and Methods*, Fig. S2) can prove that the phase shift of the mirror symmetry lines $\phi_N = \theta_1 - \theta_2 + 2\pi p/N$, $(p \in \mathbb{Z})$ depends only on the fold number as $\phi_N = \pi/N$ (*N* odd) and $\phi_N = 0$ (*N* even) and is a general consequence of *N*-fold symmetry.

The optimal rotational configuration occurs when the EET rate $|J|^2_{12}$ is maximized and is shown in Fig. 3*C*. Interestingly, the optimal configuration displays rotational and point symmetry about and through the point *O*. Placing the centers of three ninefold rings at the vertices of an equilateral triangle, we maximize $|J|^2_{3\mathrm{rings}} = |J|^2_{12} + |J|^2_{23} + |J|^2_{31}$ by rotating all three rings about their centers. The optimal rotational configuration, for which $|J|^2_{3\mathrm{rings}}$ attains a maximum, is presented in Fig. 4*A*. We find $|J|^2_{12} = |J|^2_{23} = |J|^2_{31} = 462\ \mathrm{cm}^{-2}$. Furthermore, the optimal rotation angles are all equal; i.e., $\theta_1 = \theta_2 = \theta_3 = 4°$. Noting that the ninefold ring has $S = 3$ matching points, we see that the optimal configuration in Fig. 4*A* has a rotational symmetry of order 3 with respect to the central point *O*. Consequently, the three ninefold rings constitute a triangle basis cell (Fig. 4*A*, dashed line) with the central point *O* forming a Bravais lattice [all points *O* have position vectors of the form $\vec{R} = p\vec{a} + q\vec{b}$, $(p, q \in \mathbb{Z})$, where $\vec{a}$ and $\vec{b}$ are the primitive vectors shown in Fig. 4*B*].

We can use this result, namely the existence of a basis cell, to extend the optimal rotational configuration to the entire hexagonal lattice as shown in Fig. 4*B*, where the lattice primitive cell is a hexagon. As a result of the equal angles of the optimal rotational configuration, the boundary rates of the basis cell (indicated by the 12 solid lines, joining the nearest centers) are all equal.

Eightfold B850 Rings. For two eightfold rings (Fig. S3) with $d_c = 75$ Å, the maximum coupling is $|J|^2_{12\mathrm{max}} = 315.7\mathrm{cm}^{-2}$ and the dependence of $|J|^2_{12}$ on θ_1 and θ_2 is $2\pi/8$ periodic. Note that the phase shift of the mirror symmetry line is $\phi_8 = 0$, because *N* is even. Now, in contrast to the ninefold case, the optimal

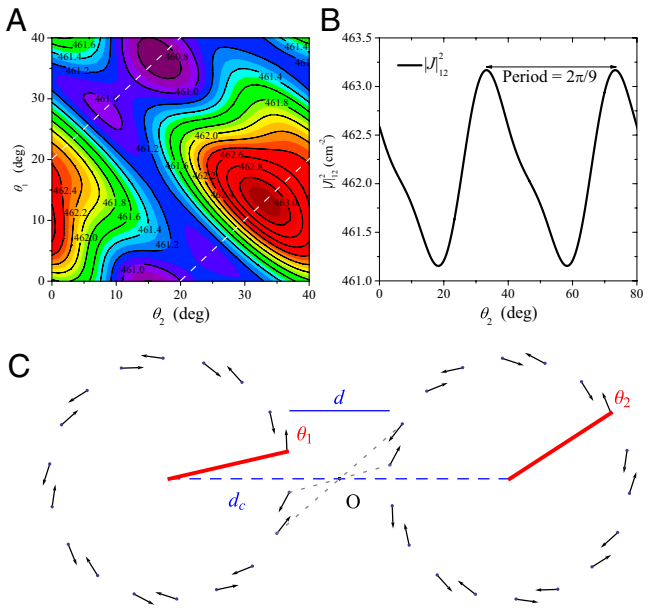

Fig. 3. (*A*) EET rate surface $|J|^2_{12}$ between two ninefold B850 rings as a function of θ_1 and θ_2. (*B*) Cross section of the surface in *A* for $\theta_1 = 13°$. A maximum is attained at $\theta_2 = 33°$. (*C*) The optimal rotational configuration has rotational and point symmetry about and through the point *O*.

rotational configuration of three eightfold rings placed at the vertices of a triangle occurs for all unequal angles, $\theta_1 \neq \theta_2 \neq \theta_3$. Hence, we consider four rings placed at the vertices of an equilateral rhombus and maximize $|J|^2_{4\text{rings}} = |J|^2_{12} + |J|^2_{23} + |J|^2_{31} + |J|^2_{14} + |J|^2_{42}$. The optimal rotational configuration is presented in Fig. S4*A*. We find a maximum EET rate for $|J|^2_{12} = 315.7$ cm^{-2}, $|J|^2_{23} = |J|^2_{14} = 314.74$ cm^{-2}, and $|J|^2_{31} = |J|^2_{42} = 314.72$ cm^{-2}.

Maximum EET now occurs at angles $\theta_1 = \theta_2 = 16°$ and $\theta_3 = \theta_4 = 39°$ so that, noting that the eightfold ring has $S = 2$ matching points, the optimal rotational configuration has a rotational symmetry of order 2 with respect to its central point *O*, which forms a Bravais lattice, where the basis cell is the equilateral rhombus (Fig. S4*B*). The boundary rates for the rhombus cell are given in Fig. S4*B*, *Right*. Unlike the ninefold case, where all-equal angles gives rise to optimized transfer rates between basis cells, the presence of two different angles within the eightfold basis cell gives rise to a single nonoptimized transfer rate between basis cells $|J|^2_{43'} = |J|^2_{34'}$, where the prime denotes a neighboring basis cell. As a result a degree of frustration in transfer rates is introduced across the hexagonal lattice.

***N*-Fold B850 Rings.** In an identical manner to that for the above nine- and eightfold cases, we determine the basis cell for each fold number N (the lowest fold number is $N = 2$, because $N = 1$ corresponds to a single heterodimer and has no fold symmetry). The results are presented in Table 1. Comparing columns 2 and 4, one finds that if an N-fold ring has two or more matching points S, there exists an optimal basis cell, so that the EET of the infinite hexagonal lattice can be optimized with respect to rotation. In the case that an N-fold ring has only one matching point there exists no basis cell, so that the infinite hexagonal lattice cannot be optimized. We thus establish a mechanism through which the fold symmetry can promote maximum EET: the existence of an optimal basis cell with rotational symmetry extendable to the entire hexagonal lattice for global optimization of the energy transfer.

In addition to determining the existence of a basis cell, the number of matching points also determines the type of basis cell. Comparing columns 2 and 3, there is a direct relationship between *S* and the triangle, rhombus, and single-ring basis cells. The type of basis cell affects the degree of EET frustration between basis cells throughout the lattice. This is especially apparent in the case of 9-fold symmetry, where the boundary rates of the basis cell are optimized, so that the frustration of EET rates between basis cells is completely removed. This is in contrast to the rhombus basis cell of the 8-fold and 10-fold rings, where the presence of the nonoptimized boundary rate $|J|^2_{43'}$ introduces a degree of EET frustration between basis cells. In the case that no basis cell exists, e.g., 7- and 11-fold rings, frustration exists throughout the entire lattice. We thus identify a complementary mechanism for the promotion of maximum EET: Frustration of EET rates between basis cells can be reduced or removed across the entire lattice through the type of optimal basis cell.

Using the above complementary mechanisms as selection criteria for the fold number, from Table 1 we can identify groups of consecutive fold numbers. Groups of consecutive fold numbers indicate robustness of the global optimization and minimal frustration mechanisms to fold number. Remarkably, one such consecutive group consists of the 8-, 9-, and 10-fold rings, which naturally occur in purple bacteria. Other N-fold rings forming consecutive groups are the 2-, 3-, and 4-fold rings and the 14-, 15-, and 16-fold rings (implicit of the structure of LH1 rings). We next

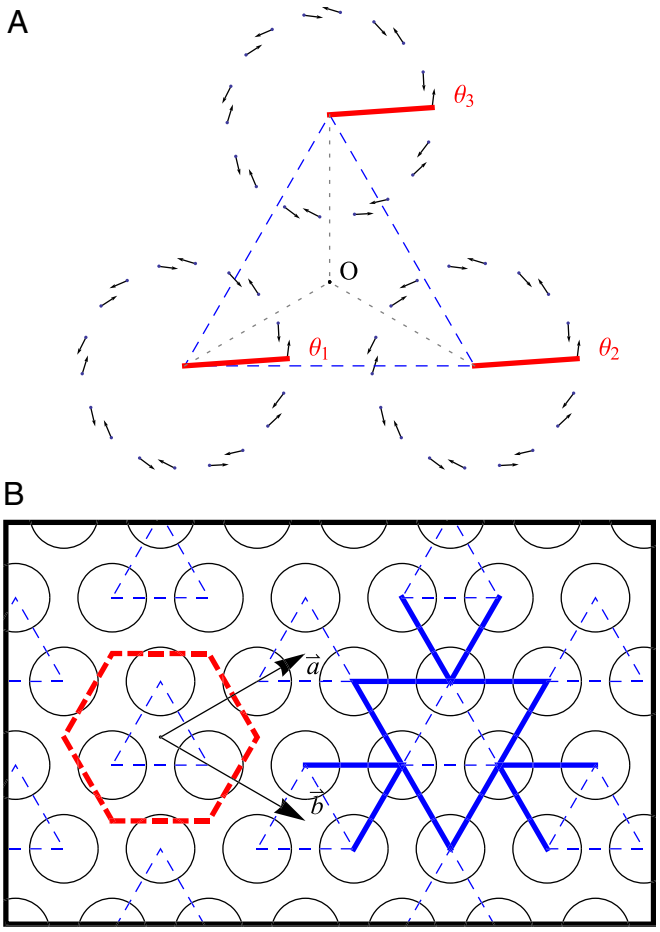

Fig. 4. (*A*) Three ninefold B850 rings placed at the vertices of the triangle basis cell (dashed line). For maximized $|J|^2_{3\text{rings}}$, both the rates between each pair and the angles of each ring are equal. Consequently the optimal rotational configuration has rotational symmetry of order 3 with respect to *O*. (*B*, *Left*) The primitive unit cell of the Bravais lattice (thick dashed line), where $\vec{a}$ and $\vec{b}$ are the primitive vectors. (*B*, *Right*) Boundary rates (12 thick solid lines) of the triangle basis cell.

Table 1. Matching points and basis cells for fold numbers 2–18

N	*S* points	Basis cell	Optimization
2	2	Rhombus	Yes
3	3	Triangle	Yes
4	2	Rhombus	Yes
5	1	None	No
6	6	Single ring	Yes
7	1	None	No
8	2	Rhombus	Yes
9	3	Triangle	Yes
10	2	Rhombus	Yes
11	1	None	No
12	6	Single ring	Yes
13	1	None	No
14	2	Rhombus	Yes
15	3	Triangle	Yes
16	2	Rhombus	Yes
17	1	None	No
18	6	Single ring	Yes

illustrate how the intermediate group of consecutive fold numbers 8, 9, and 10 may be considered preferable.

Packing Density and Rotational Sensitivity

To elucidate why 8-, 9-, and 10-fold symmetries appear preferable in nature, we extend our considerations beyond EET (relevant to the antenna network efficiency) to include the packing density ρ (relevant to the absorption cross section). For LH2 rings, the packing density can be defined as $\rho = N_H/A$, where N_H is the number of heterodimers contained in the primitive cell and A is the area of the cell. For the hexagonal lattice the primitive cell is a hexagon containing $N_H = 3N$ heterodimers with area $A = 3\sqrt{3}\, d_c^2/2$. Thus, we have

$$\rho = \frac{N_H}{A} = \frac{2N}{\sqrt{3}\, d_c^2}. \qquad [1]$$

In Fig. 5 we plot Eq. **1** (right axis, dashed line) as a function of the fold number N for the fixed inter-ring distance of the 9-fold rings $d = d_c - 2R = 21.8$ Å, where the N-dependent radius R is given in *SI Materials and Methods* (Eq. **S1**). Maintaining a fixed inter-ring distance results in a diminishing density for large fold symmetry. Alternatively, we can suppose the existence of an optimal packing density of heterodimers on the native bacterial membrane that achieves maximum absorption. To maintain this optimal packing density, the fixed-structure heterodimer subunits must self-assemble into a homogeneous N-fold ring system with a varying inter-ring distance. We choose the optimal density to be $\rho_9 \approx 1.8 \times 10^{-3}$ Å^{-2}, whereon the center-to-center distance d_c in terms of N becomes

$$d_c = \sqrt{\frac{2N}{\sqrt{3}\rho_9}} = 25\sqrt{N}. \qquad [2]$$

The inter-ring distance $d = d_c - 2R$ (left axis, solid line), where d_c is given by Eq. **2**, is shown in Fig. 5. Maintaining the criterion of an optimal packing density disallows large N-fold rings, because LH2 rings of fold number greater than 14 result in an inter-ring distance less than the physical minimum (Fig. 5, dashed line) and exceed steric contact with neighboring rings. In particular, the 14-, 15-, and 16-fold consecutive group is not possible under optimal packing density. Note an initial rise occurs in ρ and d because, for $N \leq 4$, $R \sim 21.8/2 \sim 10$ Å, respectively.

The excitation energy transfer rates and diffusion constants of the remaining consecutive groups 2-, 3-, and 4-fold and 8-, 9-, and 10-fold differ significantly. To demonstrate this we calculate the generalized Förster rate (Eq. **5**), where we must now include the spectral overlap integral (the spectral overlap differs for each fold number so that comparison of $|J|^2$ alone would be invalid). In Fig. 6 we plot the rotationally averaged transfer rate k and the corresponding diffusion constant kd_c^2 as a function of the fold number N for the cases of fixed d and ρ. In the latter (solid lines), both the transfer rate and the diffusion constant increase as N increases. In the former (dashed lines), the transfer rate k increases and then plateaus for large N (due to absence of shortening inter-ring distance), whereas the diffusion constant increases for all N. In both cases, it is preferable to have rings of larger fold number, simply to increase the absolute transfer rate and/or diffusion constant. Thus, the 8-, 9-, and 10-fold consecutive group appears preferable to the 2-, 3-, and 4-fold group.

Finally, we consider the rotational sensitivity of the energy transfer between the LH2 rings (the rotational sensitivity is indicative of the roughness of the energy landscape seen by the migrating exciton). To this end we define the percentage difference ratio, $\delta = (|J|^2_{12\max} - |J|^2_{12\min})/|J|^2_{\text{av}}$, where $|J|^2_{\text{av}} = (|J|^2_{12\max} + |J|^2_{12\min})/2$. In Fig. 7, the percentage difference ratio for EET between two rings is shown as a function of the fold number N for fixed density (solid line). As the fold number increases, the sensitivity decreases to a minimum at $N = 10$, due to the increased aggregation of the heterodimers (this is complementary to reducing the degree of frustration). For larger fold numbers $N \geq 11$, however, the effect of shortening inter-ring distance (solid line in Fig. 5) dominates increasing aggregation and the rotational sensitivity increases so that the dependence of the EET rate on dipole orientation is minimized around the 8-, 9-, and 10-fold consecutive group. The absence of this effect in the case of fixed inter-ring distance (dashed line) removes this minimum. Hence the requirements of maintaining an optimal packing density and minimal rotational sensitivity are met exclusively by the 8-, 9-, and 10-fold consecutive group.

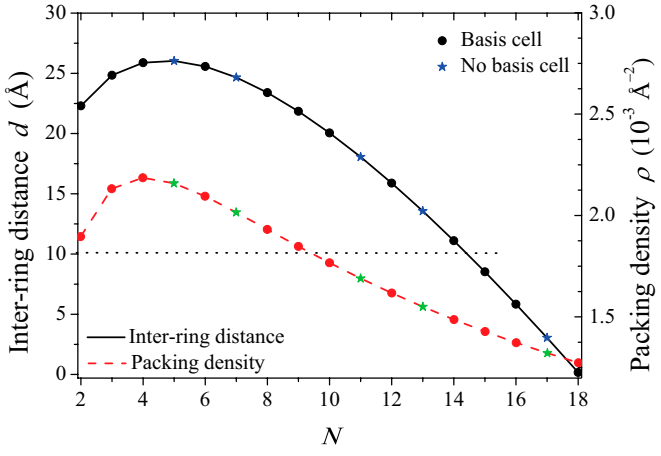

Fig. 5. Inter-ring distance d for constant density $\rho = \rho_9$ (left axis, solid line) and the packing density ρ for constant inter-ring distance $d = 21.8$ Å (right axis, dashed line) as a function of fold number N. The fold numbers for which a or no basis cell exists are indicated with a solid circle or star. The minimum physical inter-ring distance $d_{\min} = 10$ Å is indicated by the dotted line.

Discussion

We have investigated the role of the fold symmetry of LH2 in promoting maximum excitation energy transfer on the hexagonal lattice. Considering the related issues of symmetry and

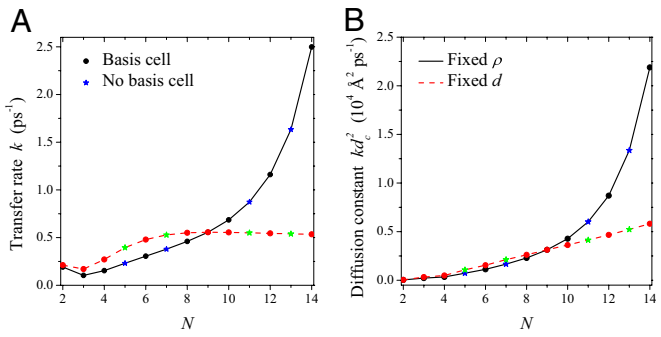

Fig. 6. (*A*) Excitation energy transfer rate k between two rings as a function of the fold number N for fixed packing density (solid line) and inter-ring distance (dashed line). (*B*) Corresponding diffusion constants kd_c^2.

frustration, we conclude that the fold symmetry can promote maximum EET via two complementary mechanisms. First, the existence of an optimal basis cell allows optimization of the entire hexagonal domain, thus enhancing the network efficiency. Second, the type of basis cell can significantly reduce or remove the degree of EET frustration between basis cells across the lattice, thus smoothing the EET landscape and enhancing robustness. EET efficiency and robustness are precisely the design criteria of a functioning light-harvesting organism, e.g., the distance over which an exciton can migrate before relaxation has a direct consequence for the ratio of LH2 to LH1/reaction center complexes (required to capture the exciton for further use) in natural systems (1–4).

A key result is that the existence of an optimal basis cell and its type are directly related to the number of matching points S. Additionally, basis cells exist for groups of consecutive fold numbers, particularly the group of naturally occurring 8-, 9-, and 10-fold rings. Considering the inter-ring distance, EET rate, and diffusion constant, we have demonstrated how this group achieves minimal rotational sensitivity in addition to an optimal packing density. Minimal rotational sensitivity and optimal packing density facilitate the biological function of a pigment–protein complex in a light-harvesting role, where essentially isotropic, delocalized behavior is desired (26). In other words, minimization of the roughness of the energy landscape allows for robust EET, whereas an optimal packing density enhances the transfer efficiency. This essentially corroborates our finding that the existence and type of an optimal basis cell achieve global optimization and minimal frustration across the hexagonal lattice and, through their direct relation to S, suggests the design principle of matching the internal symmetry of the LH complex to the underlying lattice order.

All of the above considerations provide theoretical insight into the role of fold symmetry, arising at the molecular level, in promoting efficient and robust EET at the supramolecular level of the light-harvesting antenna. Recent experiments in synthetic light harvesting (21, 22), for example, have found that hexagonal arrays of 9-fold LH2 achieve diffusion constants greatly enhanced over those observed in LH2 domains in their natural membrane due to increased coupling of the complexes. Our design principle predicts that this enhancement should be relatively reduced for 8- and 10-fold rings due to lattice mismatch and increased EET frustration. It is hoped this work will inform photosynthetic, self-assembled materials, and lithographic communities striving to understand solar light harvesting, its limits, and its design principles.

Finally, we note that increasingly sophisticated techniques continue to yield exciting discoveries at the molecular level of LH2 (27). Although we have here considered only the EET between individual LH2 complexes, thus ignoring the dynamics that occur within the complex, our qualitative conclusions should remain intact. For example, we know that neither static nor thermal disorder in an LH2 ring is strong enough to remove its excitonic characteristic, so that the main contribution to the average transfer rate between two rings still comes from the lowest (formerly) degenerate eigenstates (even with disorder a multichromophoric FRET theory between rings must be used). Furthermore, although disorder quantitatively changes the average transfer rate between two rings, the average transfer rate will still be $2\pi/N$ periodic with respect to rotation and have a mirror symmetry phase of $\phi_N = \pi/N$ (N odd) and $\phi_N = 0$ (N even) (Eq. **S7**). We thus expect our conclusions regarding the fold symmetry mechanisms to hold in the disordered scenario. The extension of our understanding of both the structure and the dynamics of individual molecular complexes to their supramolecular function presents a significant challenge for the future.

Materials and Methods

The system Hamiltonian of two B850 rings may be written

$$H = \begin{pmatrix} H_D & H_c \\ H_c^{\dagger} & H_A \end{pmatrix}, \qquad [3]$$

where H_D and H_A are the donor and acceptor Hamiltonians of the two individual rings as discussed in *SI Materials and Methods* (Eq. **S2**), H_c is the coupling Hamiltonian between the two rings $H_c = \sum_{m=1}^{N_D}\sum_{n=1}^{N_A} V_{m,n}\langle m|\langle n|$, and the inter-ring electronic coupling elements are simply $V_{m,n} = \langle m|H_c\langle n|$ and are calculated using the dipole–dipole approximation.

Now, due to the weak electronic coupling between LH2 rings, the excitation energy transfer is incoherent. Thus, the hopping rate is adequately described by the multichromophoric Förster theory

$$k = \sum_{m,m'}^{N_D}\sum_{n,n'}^{N_A} \frac{V_{m,n}V_{m',n'}}{2\pi\hbar^2}\int_{-\infty}^{\infty} E^D_{m',m}(\omega) I^A_{n,n'}(\omega)\, d\omega, \qquad [4]$$

where $E^D_{m',m}(\omega)$ and $I^A_{n,n'}(\omega)$ are the site basis elements of the donor emission and acceptor absorption spectra; i.e., $E^D_{m',m}(\omega) = \langle m'|E_D(\omega)|m\rangle$ and $I^A_{n,n'}(\omega) = \langle n|I_A(\omega)|n'\rangle$. The diffusion constant of excitons between rings is simply kd_c^2, where d_c is the ring center-to-center distance. Now if we use the diagonal (secular) approximation in the eigenstate basis of the donor and acceptor

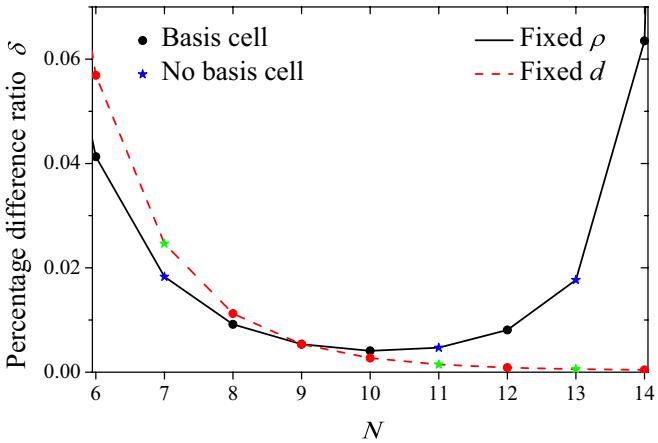

Fig. 7. Percentage difference ratio δ as a function of the fold number N for fixed density ρ (solid line) and fixed inter-ring distance d (dashed line). As the fold number increases, the rotational sensitivity obtains a minimum for 10-fold symmetry.

systems so that $\langle \varepsilon_\mu^D | E_D(\omega) | \varepsilon_{\mu'}^D \rangle = E_\mu^D(\omega)\delta_{\mu,\mu'}$ and $\langle \varepsilon_\nu^A | I^A(\omega) | \varepsilon_{\nu'}^A \rangle = I_\nu^A(\omega)\delta_{\nu,\nu'}$, we have the diagonal multichromophoric Förster rate

$$k = \frac{1}{2\pi\hbar^2} \sum_{\mu}^{N_D} \sum_{\nu}^{N_A} \left| \sum_{m=1}^{N_D} \sum_{n=1}^{N_A} V_{m,n} C_\mu^m C_\nu^{n^*} \right|^2 \times \int_{-\infty}^{\infty} E_\mu^D(\omega) I_\nu^A(\omega) d\omega, \quad [5]$$

often referred to as the generalized Förster rate. Clearly excitation energy transfer can occur between two rings via any pair of eigenstates $|\varepsilon_\mu^D\rangle$ and $|\varepsilon_\nu^A\rangle$. However, noting that most of the total oscillator strength of a single ring is contained in its lowest degenerate eigenstates $|\varepsilon_2\rangle$ and $|\varepsilon_3\rangle$, we simplify our calculation by considering only excitation energy transfer between these two eigenstates so that we need only count the four terms given by $\mu = 2, 3$ and $\nu = 2, 3$ in Eq. **5**. Furthermore, because these eigenstates are degenerate, we have $E_2^D(\omega) = E_3^D(\omega)$ and $I_2^A(\omega) = I_3^A(\omega)$ so that the overlap integral may be factorized out. Upon translation or rotation of a ring, the spectrum does not change, and hence the contribution from the spectral overlap remains constant. Therefore, to find the optimal rotational positions of two B850 rings, we need only calculate the effective dipolar coupling term

$$\begin{aligned} |J|^2 &\equiv \sum_{\mu=2}^{3} \sum_{\nu=2}^{3} \left| \sum_{m=1}^{N_D} \sum_{n=1}^{N_A} V_{m,n} C_\mu^m C_\nu^{n^*} \right|^2, \\ &= \left| \langle \varepsilon_2^A | H | \varepsilon_2^D \rangle \right|^2 + \left| \langle \varepsilon_2^A | H | \varepsilon_3^D \rangle \right|^2 \\ &\quad + \left| \langle \varepsilon_3^A | H | \varepsilon_2^D \rangle \right|^2 + \left| \langle \varepsilon_3^A | H | \varepsilon_3^D \rangle \right|^2, \end{aligned} \quad [6]$$

where the second relation in terms of H from Eq. **3** is obtained by extending the dimension of $|\varepsilon_\mu^D\rangle$ and $|\varepsilon_\nu^A\rangle$ from $2N$ to $4N$ by adding zeros at the end and beginning of the eigenvectors, respectively.

ACKNOWLEDGMENTS. This work was supported by the National Science Foundation (Grant CHE-1112825) and the Defense Advanced Research Planning Agency (Grant N99001-10-1-4063). L.C. is supported by the Center of Excitonics, an Energy Frontier Research Center funded by the US Department of Energy, Office of Science, Office of Basic Energy Sciences under Award DE-SC0001088.

1. Fleming GR, van Grondelle R (1994) The primary steps of photosynthesis. *Phys Today* 47(2):48–55.
2. Zuber H, Cogdell RJ (1995) *Anoxygenic Photosynthetic Bacteria*, eds Blankenship RE, Madigan MT, Bauer CE (Kluwer, Dordrecht, The Netherlands).
3. Blankenship RE (2002) *Molecular Mechanisms of Photosynthesis* (Blackwell Science, London).
4. Renger T (2011) Modeling of photosynthetic light-harvesting: From structure to function. *Proc Chem* 3(1):236–247.
5. Hochstrasser RM (1966) *Molecular Aspects of Symmetry* (W A Benjamin, New York).
6. Prince SM, et al. (1997) Apoprotein structure in the LH2 complex from Rhodopseudomonas acidophila strain 10050: Modular assembly and protein pigment interactions. *J Mol Biol* 268(2):412–423.
7. Hu X, Ritz T, Damjanović A, Schulten K (1997) Pigment organization and transfer of electronic excitation in the photosynthetic unit of purple bacteria. *J Phys Chem B* 101(19):3854–3871.
8. Sundström V, Pullerits T, van Grondelle R (1999) Photosynthetic light-harvesting: Reconciling dynamics and structure of purple bacterial LH2 reveals function of photosynthetic unit. *J Phys Chem B* 103(13):2327–2346.
9. McDermott G, et al. (1995) Crystal structure of an integral membrane light-harvesting complex from photosynthetic bacteria. *Nature* 374:517–521.
10. Koepke J, Hu X, Muenke C, Schulten K, Michel H (1996) The crystal structure of the light-harvesting complex II (B800-850) from Rhodospirillum molischianum. *Structure* 4(5):581–597.
11. Janosi L, Keer H, Kosztin I, Ritz T (2006) Influence of subunit structure on the oligomerization state of light-harvesting complexes: A free energy calculation study. *Chem Phys* 323(1):117–128.
12. Miller KR (1982) Three-dimensional structure of a photosynthetic membrane. *Nature* 300:53–55.
13. Bahatyrova S, et al. (2004) The native architecture of a photosynthetic membrane. *Nature* 430(7003):1058–1062.
14. Frese RN, et al. (2004) The long-range organization of a native photosynthetic membrane. *Proc Natl Acad Sci USA* 101(52):17994–17999.
15. Scheuring S, et al. (2004) Watching the photosynthetic apparatus in native membranes. *Proc Natl Acad Sci USA* 101(31):11293–11297.
16. Gonçalves RP, Bernadac A, Sturgis JN, Scheuring S (2005) Architecture of the native photosynthetic apparatus of Phaeospirillum molischianum. *J Struct Biol* 152(3): 221–228.
17. Scheuring S, Sturgis JN (2009) Atomic force microscopy of the bacterial photosynthetic apparatus: Plain pictures of an elaborate machinery. *Photosynth Res* 102(2–3): 197–211.
18. de Rivoyre M, Ginet N, Bouyer P, Lavergne J (2010) Excitation transfer connectivity in different purple bacteria: A theoretical and experimental study. *Biochim Biophys Acta* 1797:1780–1794.
19. Olbrich C, Kleinekathöfer U (2011) From atomistic modeling to electronic properties of light-harvesting systems. *Semiconductors and Semimetals*, eds Würfel U, Thorwart M, Weber ER (Academic Press, Burlington, MA), Vol 85, Chap 3, pp 83–114.
20. Cao J, Silbey RJ (2009) Optimization of exciton trapping in energy transfer processes. *J Phys Chem A* 113(50):13825–13838.
21. Escalante M, et al. (2008) Nanometer arrays of functional light harvesting antenna complexes by nanoimprint lithography and host-guest interactions. *J Am Chem Soc* 130(28):8892–8893.
22. Escalante M, et al. (2010) Long-range energy propagation in nanometer arrays of light harvesting antenna complexes. *Nano Lett* 10(4):1450–1457.
23. Pflock TJ, et al. (2011) The electronically excited states of LH2 complexes from Rhodopseudomonas acidophila strain 10050 studied by time-resolved spectroscopy and dynamic Monte Carlo simulations. II. Homo-arrays of LH2 complexes reconstituted into phospholipid model membranes. *J Phys Chem B* 115(28):8821–8831.
24. Beyer SR, et al. (2011) Hybrid nanostructures for enhanced light-harvesting: Plasmon induced increase in fluorescence from individual photosynthetic pigment-protein complexes. *Nano Lett* 11(11):4897–4901.
25. Reuter MG, Seideman T, Ratner MA (2011) Molecular conduction through adlayers: Cooperative effects can help or hamper electron transport. *Nano Lett* 11(11): 4693–4696.
26. Fleming GR, Schlau-Cohen GS, Amarnath K, Zaks J (2012) Design principles of photosynthetic light-harvesting. *Faraday Discuss* 155:27–41, discussion 103–114.
27. Harel E, Engel GS (2012) Quantum coherence spectroscopy reveals complex dynamics in bacterial light-harvesting complex 2 (LH2). *Proc Natl Acad Sci USA* 109(3): 706–711.